Eurographics Symposium on Rendering (2007)
Jan Kautz and Sumanta Pattanaik (Editors)

Dirty Glass: Rendering Contamination on Transparent Surfaces

Jinwei Gu, Ravi Ramamoorthi, Peter Belhumeur, Shree Nayar

Columbia University

Abstract

Rendering of clean transparent objects has been well studied in computer graphics. However, real-world transparent objects are seldom clean—their surfaces have a variety of contaminants such as dust, dirt, and lipids. These contaminants produce a number of complex volumetric scattering effects that must be taken into account when creating photorealistic renderings. In this paper, we take a step toward modeling and rendering these effects. We make the assumption that the contaminant is an optically thin layer and construct an analytic model following results in radiative transport theory and computer graphics. Moreover, the spatial textures created by the different types of contamination are also important in achieving visual realism. To this end, we measure the spatially varying thicknesses and the scattering parameters of a number of glass panes with various types of dust, dirt, and lipids. We also develop a simple interactive synthesis tool to create novel instances of the measured contamination patterns. We show several results that demonstrate the use of our scattering model for rendering 3D scenes, as well as modifying real 2D photographs.

Categories and Subject Descriptors (according to ACM CCS): I.3.7 [Computer Graphics]: Three-Dimensional Graphics and Realism

1. Introduction

In our daily lives, we are surrounded by transparent surfaces such as windows, windshields, monitors, reading glasses, drinking glasses, camera lenses, and mirrors. The rendering of the effects produced by clean transparent surfaces has been widely studied, and today's advanced rendering techniques [Jen01] are able to accurately and efficiently render the most salient effects. However, rendered images of clean transparent surfaces tend to look too perfect. As seen in real photographs in Fig. 1, transparent objects almost always have surface contaminants such as dust (e.g., pollen, skin cells, fabric fibers), dirt (e.g., powder, salt, other minerals, organic materials, soil), and lipids (e.g., fingerprints, lipstick, and other oils). These imperfections produce weathered appearances critical to achieving realism in rendered images [DH00].

At first glance, it may seem that simply alpha-blending a contaminant layer over the transparent surface is adequate. However, the scattering, attenuation, and occlusion due to a contaminant layer can produce striking visual effects. For example, in Fig. 1a the dirt looks darker against the sky on the top, while it looks brighter against the ground on the bottom. In Fig. 1b, the stains on the wine glass alter the light transport through the surfaces and create an interesting soiled appearance. Dust on a camera lens scatters light from outside the field of view of the lens to the image detector to produce lens glare, as shown in Fig. 1c. Fingerprints or other contaminants become clearly visible on a monitor screen when the monitor is off, as seen in Fig. 1d. The visual effects also vary dramatically with viewing and illumination angles. For instance, contaminants on glass that are barely visible in a frontal view become clearly visible when viewed from a grazing angle.

To model the light transport for contaminated transparent surfaces, we consider the contaminant to be a thin layer of a scattering medium over a smooth transparent surface. Our model follows directly from the layered subsurface scattering models in the literature on radiative transport theory [Cha60, Ish78] and is closely related to the layered surface model of Hanrahan and Krueger [HK93]. To construct our model, we modify [HK93] to include additional terms

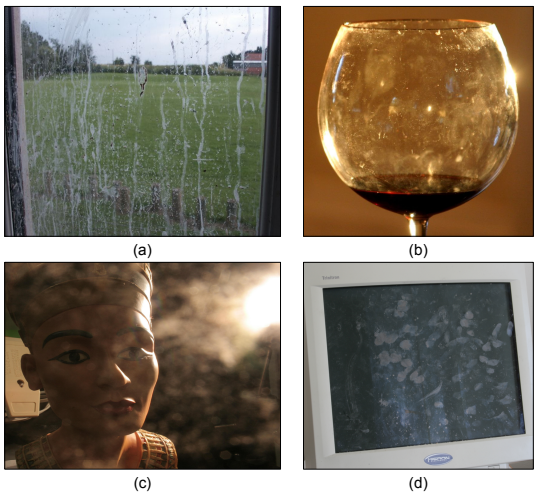

Figure 1: *Real photographs of scenes with transparent objects. (a) Window with dirt; (b) wine glass with stains; (c) image taken with a dusty lens; and (d) monitor with fingerprints. Contaminants on the transparent objects produce many striking visual effects.*

as needed (see Sec. 3). The final model includes reflection at the air-contaminant interface and the scattering of the light reflected from the contaminated transparent surface. In Sec. 4, we show that the model captures many of the canonical visual effects common in the real world, such as the contrast reversals (i.e., darker/brighter) of the contaminated regions against the background, lens flare/blurring caused by stray light, and the angular dependency with the viewing/lighting direction (i.e., increased scattering at grazing angles (Fig. 15) and the vertical "shadow" (Fig. 17a)).

In rendering contamination effects, we must also consider the spatial distribution or "texture" of the contaminant. To this end, we have developed methods for measuring the spatial pattern and scattering parameters of a contaminant layer on a thin sheet of glass or plastic (Sec. 5). To acquire the spatial pattern, we use a projector to illuminate the sheet from one side and create a shadow of the pattern on a Lambertian surface placed on the other side. From a single image of the shadow map of the pattern, we estimate the spatially varying thickness of the contaminant. To measure the scattering parameters, we use a thin collimated light beam to scatter light through the layer onto a Lambertian surface placed a small distance behind. From this second image, we estimate the scattering parameters for a given contaminant type. To date, we have measured the patterns and scattering parameters of 30 transparent sheets contaminated with dust, dirt, and lipids. These measurements have been incorporated into a simple interactive tool that uses texture synthesis to generate a contaminant layer of any desired size, with user-selected combinations of contaminant types. Our database of measured contaminants and the synthesis tool will be available at http://www.cs.columbia.edu/CAVE.

The BRDF/BTDF model and measurements can be plugged directly into a renderer to generate the appearance of a variety of contaminants on different types of transparent surfaces. In Sec. 6, we show rendered images of 3D scenes (Figs. 13-17) that include all the effects seen in Fig. 1. We also show how our model can be used to add contamination effects to 2D photographs (Figs. 18-20).

2. Previous Work

Weathering of Surfaces: In recent years, modeling and rendering of the weathered appearance of surfaces has received significant attention, going back to the work on modeling patina formation and flows by [DH96, DPH96]. Recent work based on physical simulation and surface geometry includes [Mil94, HW95, DEWJ*99, MDG01, PPD01]. Most recently, a data-driven approach has been used to model the time-varying nature of appearance [WTL*06, GTR*06]. Another body of work addresses how defects such as scratches change surface reflectance [BPMG04] or how wetness or dust change reflectance of opaque materials [LGR*05, SSR*06].

While these papers focus on weathering or time-varying effects on opaque objects, our focus is on the appearance of thin layers of contaminants on transparent surfaces. These previous works do not address the volumetric scattering and transmission effects that are critical in our case.

Modeling of Thin Scattering Layers on Surfaces: Blinn [Bli82] derived a model for an opaque surface covered with a thin layer of dust, based on the assumption of single scattering. Koenderink and Pont [KP03] derived a similar simplified model and found that it is the outer scattering layer that causes the smooth and velvety appearance of many soft materials like peaches and cloth.

To our knowledge, [HK93] is the first work in computer graphics which systematically studied light transport for layered materials due to subsurface scattering. Based on results from radiative transport theory [Cha60, Ish78], they derived analytic models for single scattering and developed an algorithm for Monte Carlo simulation for multiple scattering. Pharr and Hanrahan [PH00] and Ershov et al. [EKM01] developed a recursive procedure to extend the analytic models for one layer to multiple layers for the purpose of interactive rendering of paint-composition materials (e.g., pearlescent paints) or simulation of multiple scattering effects.

In this paper, we consider a specific type of layered material—a thin contaminant layer on a transparent surface. In addition to the scattering events modeled in the previous work [HK93], our specific problem has its own set of scattering events. In particular, these events include reflection at the air-contaminant interface and the scattering of the light reflected from the contaminated transparent surface. Our model for contaminated transparent surfaces includes additional terms for handling these light transport events.

Diffusion Model in Subsurface Scattering: Our work is also related to the diffusion model [JMLH01] for subsurface scattering. Stam [Sta01] proposed a semi-analytic

	Interface with Air	Optical Thickness	Scattering
Dust	No, $n_1 = n_2$	Small	$0.4 \le g \le 0.9$
Dirt	Yes, $n_1 \neq n_2$	Medium	$0 \le g \le 0.8$
Lipids	Yes, $n_1 \neq n_2$	Small	$0.7 \le g \le 1$

Figure 2: *Definitions of the three types of contaminants.*

model for multiple anisotropic scattering in a layer bounded by two rough surfaces. Our problem is simpler. The contaminant layer on transparent surfaces is usually optically thin so that single scattering rather than diffusion dominates. Also, unlike subsurface scattering in an optically thick medium [JMLH01], the spatial transport of light in the contaminant layer need not be considered.

Measurement of Scattering Parameters: In both physics and computer graphics, there is much previous work on measuring the scattering parameters for various kinds of materials, such as minerals [WDE*97], tissues [CPW90], and liquids [JDJ06, NGD*06, HM03]. Nevertheless, there appear to be few existing measurements for the kinds of contamination, such as dust, lipstick, soap stains, etc., relevant to the models in this paper. This is partially because of the complexity of the measurement. Usually it requires specialized equipments (e.g., scatterometer) or special procedures only suitable for limited types of materials (e.g., dilution of liquid [NGD*06]). In this paper, we develop a rather simple method to measure the scattering parameters for various kinds of contamination based on the BRDF/BTDF model, which requires only a single image and can be easily implemented.

3. Modeling of Light Transport

In this section, we construct our model for light transport on a contaminated transparent surface. Our model can be seen as a modification to the layered surface model in [HK93]. For completeness, we detail all the terms in our model below.

In Fig. 2 we loosely define three categories of contaminants—dust, dirt and lipids. The thresholds for the scattering parameter g are determined conservatively from the physics literature [Dra03, JDJ06, SFMM01] and our own measurements in Sec. 5.2. An important observation is that most of the contaminant layer is optically very thin, either because it is physically thin (such as a lipid layer), or because its density is low (such as dust). Therefore we assume that single scattering dominates and aggregate the scattering events to a local BRDF/BTDF model. As shown in Fig. 4a, for the light $L_i(\omega_i)$ incident from the air onto the transparent medium, i.e., $\omega_i \cdot N > 0$, there are 4 components for reflection and 2 components for transmission, each of which has been derived previously in [Cha60, Ish78]. Notation for selected symbols are shown in Fig. 3.

3.1. Construction of the BRDF/BTDF Model

Mirror Reflection from the Contaminant Surface $L_r^{(1)}(\omega_r)$: If the contaminant layer has an interface with the air ($n_1 \neq n_2$), we will have a mirror-reflection at the surface of the contaminant, and

L_i	Incident light radiance
L_r	Reflected light radiance
L_t	Transmitted light radiance
ω_i	Incident light direction (θ_i, ϕ_i), $\mu_i = \cos\theta_i$
ω_r	Reflected light direction (θ_r, ϕ_r), $\mu_r = \cos\theta_r$
ω_t	Transmitted light direction (θ_t, ϕ_t), $\mu_t = \cos\theta_t$
N	Surface normal
F_{12}	Amount of light reflected at air-contaminant interface
F_{23}	Amount of light reflected at contaminant-glass interface
T_{12}	Amount of light transmitted from air to contaminant
T_{23}	Amount of light transmitted from contaminant to glass
n_1	Refractive index of air
n_2	Refractive index of the contaminant
n_3	Refractive index of glass (transparent medium)
τ	Optical thickness of the contaminant layer
ϖ_0	Albedo of the contaminant for single scattering
g	Mean cosine of the scattering angle
$p(\theta)$	Phase function
$f_r(\omega_i, \omega_r)$	BRDF of the contaminated transparent surface
$f_t(\omega_i, \omega_r)$	BTDF of the contaminated transparent surface

Figure 3: *Notations for the main quantities used in the paper.*

$$L_r^{(1)}(\omega_r) = F_{12} \cdot \delta(\omega_i, \omega_r) \cdot L_i(\omega_i), \quad (1)$$

where F_{12} is the Fresnel term for reflection [HK93], and $\delta(\omega_i, \omega_r)$ is the delta function.

Mirror Reflection from the Transparent Surface $L_r^{(2)}(\omega_r)$: This component models the light that makes it through the contamination layer to the transparent surface and then is mirror reflected back toward the contaminant layer. As the light travels inside the contaminant layer it is attenuated exponentially with the optical path depth, leaving the *reduced intensity* [Ish78]. Notice that the light will be attenuated twice—when it is transmitted into the contaminant and when it is reflected back. This yields

$$L_r^{(2)}(\omega_r) = e^{-\tau(\frac{1}{\mu_i'} + \frac{1}{\mu_r'})} \cdot T_{12} T_{21} F_{23} \cdot \delta(\omega_i, \omega_r) \cdot L_i(\omega_i), \quad (2)$$

where τ is the optical thickness of the contaminant layer, ω_i' and ω_r' are the directions of the refracted rays in the contaminant layer computed by Snell's law (see Fig. 4a), and μ_i' and μ_r' are the cosine of their zenith angles θ_i' and θ_r'. Since we consider mirror reflection, $\omega_i' = \omega_r'$. T_{12} and T_{21} are Fresnel terms for transmission [HK93].

Scattering of the Incident Light $L_r^{(3)}(\omega_r)$: This component is due to scattering and is called the *diffuse intensity* [Ish78]. Under the single scattering assumption, it is given by

$$L_r^{(3)}(\omega_r) = \frac{T_{12} T_{21} \mu_i'}{\mu_i' + \mu_r'} \cdot \left(1 - e^{-\tau(\frac{1}{\mu_i'} + \frac{1}{\mu_r'})}\right) \cdot \varpi_0 p(\pi - \theta_i' - \theta_r') \cdot L_i(\omega_i). \quad (3)$$

where $p(\theta)$ is the scattering function (phase function), ϖ_0 is the *albedo for single scattering* [Cha60] of the contaminant.

Scattering of the Mirror-reflected Light $L_r^{(4)}(\omega_r)$: Like the previous term, this term involves single scattering of the light reflected from the transparent surface (bottom lit):

$$L_r^{(4)}(\omega_r) = \frac{T_{12} T_{21} F_{23} \mu_i'}{\mu_i' - \mu_r'} \cdot \left(e^{-\frac{\tau}{\mu_i'}} - e^{-\frac{\tau}{\mu_r'}}\right) e^{-\frac{\tau}{\mu_i'}} \cdot \varpi_0 p(\theta_i' - \theta_r') \cdot L_i(\omega_i). \quad (4)$$

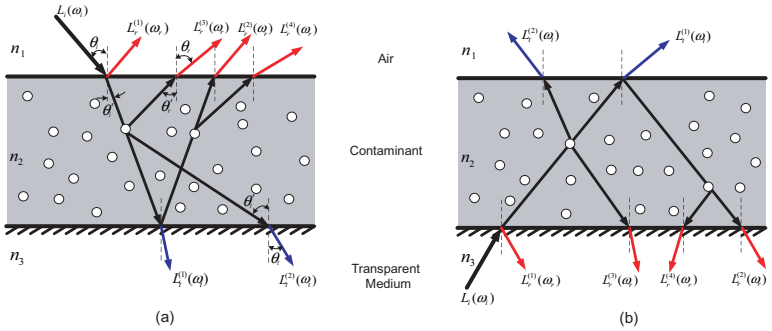

Figure 4: *Light transport for a contaminated transparent surface: (a) Incident light from air to transparent medium; (b) from transparent medium to air.*

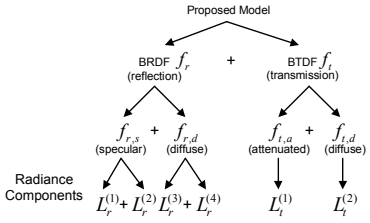

Figure 5: *Relationship of the model and individual components.*

Transmission of the Incident Light $L_t^{(1)}(\omega_t)$: This component models the light that makes it through the contaminant layer and is transmitted into the transparent surface:

$$L_t^{(1)}(\omega_t) = e^{-\tau/\mu_i'} \cdot T_{12}T_{23} \cdot \delta(\omega_i', \omega_t') \cdot L_i(\omega_i), \qquad (5)$$

where ω_t' is the direction of the ray before it is refracted into the transparent surface as computed from ω_t by Snell's law.

Scattering of the Incident Light $L_t^{(2)}(\omega_t)$: This component models the light scattered into the transparent surface:

$$L_t^{(2)}(\omega_t) = \frac{T_{12}T_{23}\mu_i'}{\mu_i' - \mu_t'} \cdot \left(e^{-\tau/\mu_i'} - e^{-\tau/\mu_t'}\right) \cdot \varpi_0 p(\theta_i' - \theta_t') \cdot L_i(\omega_i). \qquad (6)$$

Summary: From all the above components, the actual BRDF/BTDF model can be obtained by dividing the components by the cosine-weighted incident light $L_i(\omega_i)\mu_i$ and summing them. As shown in Fig. 5, the resulting BRDF model will have both a specular or mirror term $f_{r,s}$ (coming from $L_r^{(1)}$ and $L_r^{(2)}$) as well as a diffuse component for scattered light $f_{r,d}$ (coming from $L_r^{(3)}$ and $L_r^{(4)}$). The BTDF will have both the attenuated term $f_{t,a}$ (from $L_t^{(1)}$) as well as the diffuse term $f_{t,d}$ (from the scattering $L_t^{(2)}$). Similar results are derived in the Appendix for the case when $\omega_i \cdot N < 0$, i.e., light incident from the transparent surface to the air.

Comparison: Many of the components above overlap with the models in [HK93,Bli82]. However, there are components which are in our model while not in [Bli82] (i.e., $L_r^{(1)}$, $L_r^{(2)}$, $L_r^{(4)}$) and [HK93] (i.e., $L_r^{(2)}$ and $L_r^{(4)}$). These additional components are used to model certain light transport events important for contaminated transparent surfaces, such as rendering certain kinds of contamination (e.g., lipids and dirt) or rendering under certain lighting or view conditions (e.g., stray light or viewing at grazing angles).

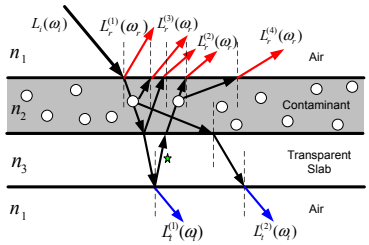

Figure 6: *Light transport for a thin transparent slab with contamination, where the incident light goes from air into the slab and again into air. This is a special case of our model.*

Following others, we use the Henyey-Greenstein phase function for $p(\theta)$. Thus, there are 4 input parameters in the model (assume n_1 and n_3 are known and fixed): τ, the optical thickness of the layer, usually is a texture of the contaminant pattern; g, the parameter of the Henyey-Greenstein phase function; ϖ_0, the albedo of the contaminant; and n_2, the refractive index of the contaminant. Different kinds of contaminants, such as dust, lipid/fingerprints, water deposit, powder, salt, dirt, etc., will have parameters in different ranges, while their effects are captured with the same model.

Thin Transparent Slab with Contamination: The above BRDF and BTDF model can be plugged into any raytracer to render the effects of contaminants on arbitrary transparent surfaces. However, many transparent objects in the real world are made of thin slabs which have two parallel interfaces with air, such as glass windows. To render these objects at the scales where the thickness of the slab does not need to be taken into account, we can further simplify the above BRDF/BTDF model, since both the direction and the position of the incoming ray and the outgoing ray will not change. This is essentially a combination of the above model and the model for a clean transparent surface. If both sides of the slab have contaminants, we can also combine the above model twice to get a simplified model, each of which is for one side of the slab. As shown Fig. 6, all the components can be derived similarly as above and assembled together. Details are given in the Appendix.

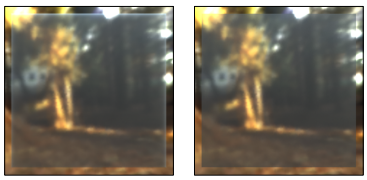

Figure 7: *A uniform layer of dust rendered with (a) brute force Monte Carlo volumetric scattering and (b) our proposed BRDF/BTDF model. Our model generates accurate results, while being much more efficient for rendering.*

Verification of Accuracy: In Fig. 7, we verify the accuracy of our BRDF/BTDF model by rendering (with a global illumination renderer) a simple scene of a dusty glass slab. Figure 7a is rendered using Monte Carlo simulation with 2048 samples per pixel needed to reduce noise, taking about 1 hour. Figure 7b uses our BRDF/BTDF model, and is rendered with 4 samples per pixel, taking about 10 seconds (this is essentially the same time as using other analytic BRDF models such as Torrance Sparrow). The RMS relative difference between these two images is 2.2%, which shows the accuracy of our model.

4. Canonical Visual Effects

In Fig. 8, we present a set of canonical examples corresponding closely to common real-world situations; in each a contaminant layer is placed on the surface of a thin transparent slab. The two leftmost columns describe the various viewing and illumination conditions considered here, as well as the placement of the contaminant layer. On the transparent slab, there are 2×3 patches of contaminants, as seen in the renderings in the rightmost column. From left to right, the contaminants are dust, dirt, and lipids (e.g., fingerprints). These three kinds of contaminants cover a large range of the parameters and are selected to demonstrate the typical effects. The two patches in each column are identical. For dust and dirt, the optical thickness of the patches are uniform; for fingerprints, we crop a fingerprint texture and use it as the optical thickness. Finally, the middle column of Fig. 8 shows scattering diagrams, with the red components being reflection and the blue components being transmission. Moreover, at the end of this section we describe the effects due to the angular dependency of the model with the viewing/lighting direction.

View of Window in Daytime: In the first row of Fig. 8, we simulate the case when we are in a dark room and look through the window outwards in daytime. Only the top region (or "sky") of the environment is (uniformly) bright. In the renderings, the upper half is bright and the bottom half is dark since only the upper half has environment light. However, the contaminated patches in the upper half look *darker* because of attenuation. By contrast, the contaminated patches (dust and fingerprints) in the bottom half look *brighter* because of scattering of the environment light. The dirt patches behave almost completely like an attenuator, with minimal scattering (consider the blue lobe in the middle scattering diagram). Therefore, that patch is black in both upper and lower regions. Similar effects can be seen in real photographs (Fig. 1a) and in rendering results (Fig. 14 and Fig. 20), where the contaminant looks darker against the sky, and brighter against the ground.

View of Window in Nighttime: The second row of Fig. 8 corresponds to the situation when we are in a bright room (the upper half is lit) and look through the window in nighttime. Unlike the previous case, the contaminants in the upper half will look *brighter* than the clean regions, because there is not only reflection from the slab but also scattering from the contaminant. The contaminants in the bottom half will also look *brighter* because of scattering. This is true even for dirt–while the light transmitted through the window is attenuated as before, in this case we see primarily the light reflected from dirt. Figure 14c shows this effect in rendering.

Monitor Turned Off: The third row in Fig. 8 mimics the situation in which a computer monitor is turned off. Note that the contaminant is on the other side, the side closer to the camera. In this case, the contaminated regions in the bottom half still look brighter than the background due to scattering. The contaminants in the upper half look slightly darker than before because the reflected light from the monitor screen will be attenuated by the contaminant before it comes to the camera. As the rendering results in Fig. 15 (and the photograph in Fig. 1d) show, the contaminant patterns are visible on the monitor when it is turned off.

Monitor Turned On: When the monitor is turned on, as shown in the fourth row in Fig. 8, there is another textured area light source behind the screen (i.e., the light from the monitor itself) in addition to the environment light. The area light is so close to the slab that the attenuated flux from the area light is much stronger than the flux scattered from the environment. Therefore, the difference between the clean regions and the regions with dust and fingerprints is not obvious, i.e., the contaminants are almost invisible. For dirt, since its optical thickness is larger, its brightness will be attenuated more and thus it appears dark like an occluder.

Collimated Beam from the Side: The fifth row in Fig. 8 mimics the scenario of sunlight striking a window or lens. In this case, a collimated beam is incident on the transparent slab from the side. The camera sees no light from the collimated beam (e.g., sunlight) in the clean regions because the transmission does not change the incident direction. In contrast, in the contaminated regions, the scattering due to the contaminants will redirect some of the light toward the camera. This is one of the reasons why a camera with a dirty lens or filter usually generates lens flare or a washed-out effect when there is strong stray light. For example, Fig. 1c and Fig. 18 show photographs taken with a dirty lens and the corresponding rendering result.

Angular Dependency with Viewing/Lighting: One common effect of contaminated transparent surfaces is that they

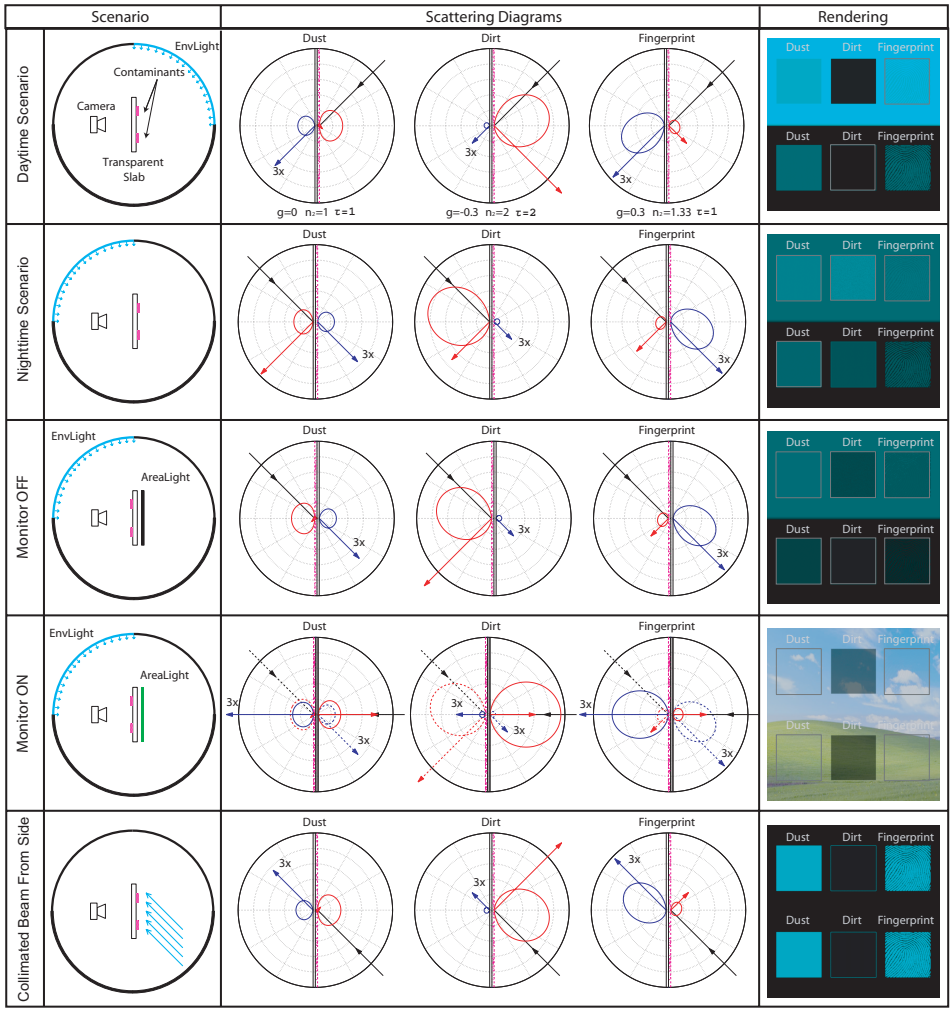

Figure 8: *Visual effects predicted by our model, illustrated for a set of canonical scenarios common in the real world. See text for details.*

are view-dependent. For example, if we look at a patch of dust on a glass pane, its appearance changes dramatically as the view changes from perpendicular angles to more grazing angles. This is caused by two factors: the Fresnel effect of the glass, i.e., at more grazing angles there is more reflected light; and the angular dependency of $f_{r,d}$ in the BRDF. This effect is shown in both the real photograph (Fig. 1b) and our renderings (Fig. 17a and Fig. 15). Moreover, Fig. 17a also shows the vertical "shadow" and the "shading" on the cognac glass. This effect, caused by the scattering of the contaminants, is both view- and lighting-dependent and is consistent with real world experience.

5. Measurement

There exist a large variety of contaminants on transparent surfaces. These contaminants can be described both by the spatial distribution of the contaminant and by the scattering properties of the contaminant type. In this section, we detail our method for measuring the optical thickness $\tau(x,y)$ and the scattering parameter g for real examples of contamination. For n_2 and ϖ_0, we choose their values either from certain manuals [Sto90] or user input. To date, we have gathered 30 examples of representative materials, including many examples of dust, dirt, and lipids. All of our gathered data, as well as a simple interactive tool for synthesizing new contamination layers will be released online.

5.1. Optical Thickness

To measure the spatial pattern of thickness or "texture" $\tau(x,y)$, we use the shadow map generated by attenuation from the contaminant layer. Figure 9a shows our setup. The projector illuminates a thin glass slab with contaminants on the far side. Behind it is a Lambertian board, and the camera is on the side. The camera is radiometrically calibrated beforehand. The intensity of each point in the shadow map comes from two parts: the attenuated transmitted light $L_t^{(1)}$ (Eq. 5) from this point, and the scattering component $L_t^{(2)}$ (Eq. 6) from neighboring points. Since the albedo of the contaminant layer is assumed to be small (otherwise it would

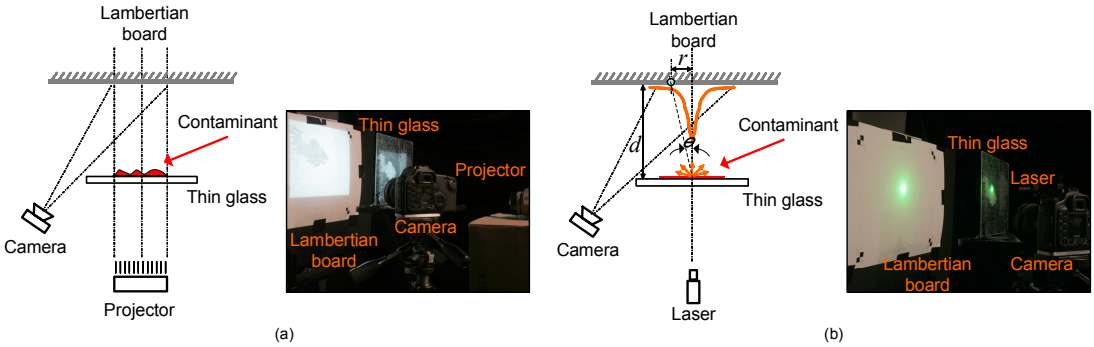

Figure 9: *Setups used to measure (a) the optical thickness $\tau(x,y)$ and (b) the scattering parameter g of a contaminant.*

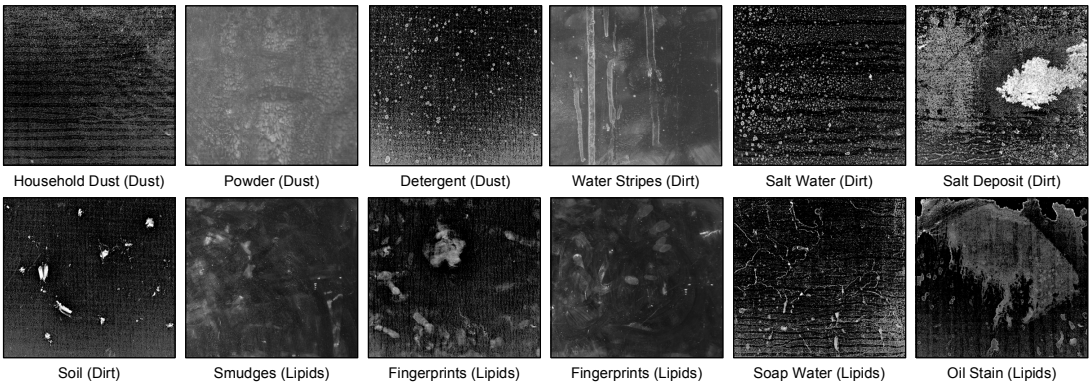

Figure 10: *Examples from 30 contamination patterns, measured with the setup in Fig. 9a. Intensity is proportional to $\tau(x,y)$.*

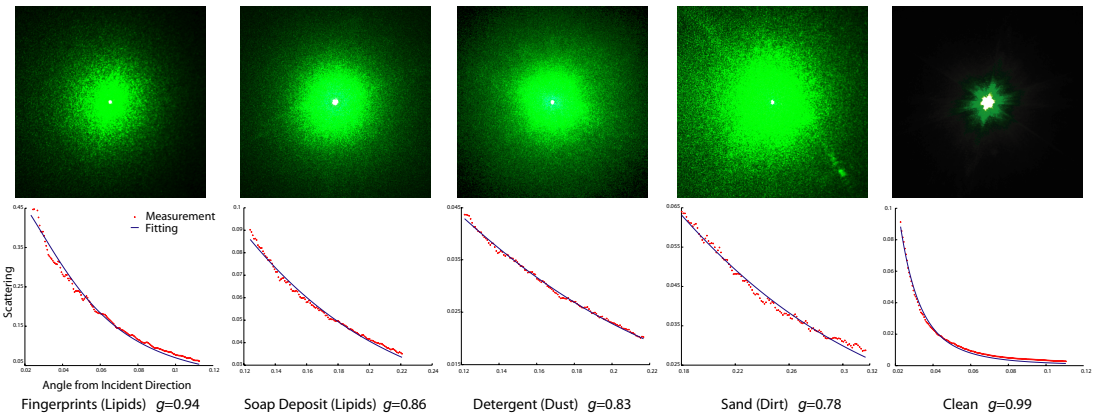

Figure 11: *Examples of images acquired using the setup in Fig. 9b for measuring the scattering parameter g.*

generate multiple scattering) and it is mostly forward scattering, there will be much less contribution from neighboring points due to scattering. Thus $L_t^{(1)}$ is much stronger than $L_t^{(2)}$ and it is the intensity of the shadow map. Based on Eq. 5, the intensity of point (x,y) in the shadow map is attenuated by $e^{-\tau(x,y)}$ ($\mu_i' = 1$ since illumination is head on). Note that the attenuation is only related to $\tau(x,y)$ and is independent of the scattering parameter g. The formula used to compute $\tau(x,y)$ is as follows:

$$\tau(x,y) = -\ln\frac{I(x,y)}{I_{\text{clean}}}, \tag{7}$$

where I_{clean} is the image intensity in the clean regions of the glass. For some samples we can indeed observe the effect of scattering from neighboring points in the shadow map, for which the shadow map usually is blurry, especially when the board is far from the glass. In those cases, we let the projector shine light through the glass and put the camera on the other side. This setup allows us to measure $\tau(x,y)$ by scattering ($L_t^{(2)}$ in Eq. 6) and the result is then scaled by the initial measurement. Figure 10 shows some acquired textures with different kinds of contaminants. Image intensity is proportional to the optical thickness.

5.2. Scattering Parameter

We aim to obtain qualitatively correct estimates of g for different materials. As shown in Fig. 9b, the setup is similar to the previous one, except in two places. First, we use a laser instead of a projector. Second, we use a uniform contaminant layer. With the previous method, we measure the thickness of this layer. When the laser beam hits the contaminants, part of it will scatter towards the Lambertian board and generate a falloff (or lobe) pattern on the board. The center region will have a very strong spike due to the attenuated laser, while the brightness of other regions is due to the scattering $L_t^{(2)}$. Based on Eq. 6, the intensity of point (x,y) is

$$I(x,y) = \beta \cdot p(\theta;g) \cdot \frac{e^{-\tau} - e^{-\tau/\cos\theta}}{1-\cos\theta} \cdot \cos^4\theta, \qquad (8)$$

where β is a scale factor, $p(\theta;g)$ is the phase function, and θ is the angle of the scattered ray from the normal. The derivation of this formula can be found in the Appendix.

We have measured 10 samples in total which contain representative contaminants in each of the three categories (i.e., dust, dirt and lipids). For other samples, we use the g values from the corresponding category for rendering. Figure 11 shows some images for different kinds of contaminants. We also show the image we acquired for clean glass for verification, where as expected the scattering is minimal. With the assumption of isotropic scattering, each circle around the center of the image corresponds to a single angle θ. We then compute the average $I(x,y)$ in the circle, and use it to fit the phase function. The second row in Fig. 11 shows the results. The red dots are the data and the blue curves are the fit. The third row shows the fit g values.

5.3. Synthesis Tool

To increase the applicability of the acquired data, we have developed a simple tool to synthesize the contaminant patterns and scattering parameters according to a user's input. The synthesized texture, in which each channel corresponds to one kind of parameter for the contaminant, can be mapped on arbitrary transparent objects for rendering.

We first build a database by selecting a collection of prototypes for each of the three categories of contamination (dust, dirt, and lipids) from the measured data. For synthesis, as shown in Fig. 12, a user selects prototypes from each category for the desired contamination pattern and specifies the size of the output texture. For example, the desired pattern might be a combination of fingerprints or smudges, some stripes of water deposit, and a layer of dust. The tool then synthesizes a contamination layer for each prototype individually. For dust, we use image quilting [EF01] for synthesis. For lipids (fingerprints), we randomly transform (scale and rotate) the prototype and randomly tile several copies on the canvas. For dirt, we use a similar random placement but we limit the range of rotation and translation since the water stripes usually are on the top of an image. The three synthesized layers are then alpha-blended together to generate the final texture. A user can control the amount and the range of transformation for each prototype and also add/remove more prototypes interactively.

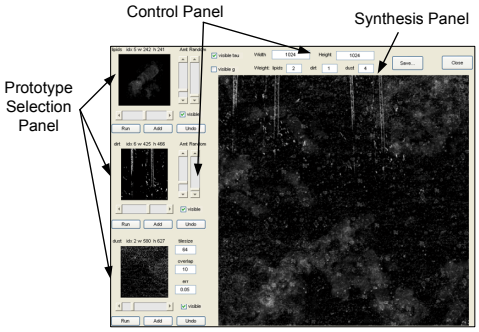

Figure 12: *Interactive synthesis tool developed to generate novel contaminant patterns from the set of measured ones.*

6. Rendering Results

We now show some rendering results of transparent objects with various kinds of contamination both in 3D scenes and on 2D photographs. In all the examples, sampling of the BRDF/BTDF models is done by sampling the Henyey-Greenstein phase function. The parameters of the contaminant layer are generated with the synthesis tool.

6.1. Rendering of 3D Scenes

We plug our BRDF/BTDF models into a physically-based ray tracer PBRT [PH04] and render with either direct lighting or global illumination algorithms.

Glass Sphere Covered with Uniform Dust: Figure 13 shows a glass sphere covered with a uniform dust layer in a complex lighting environment while the optical thickness of the dust, τ, increases. As shown, the appearance of the glass sphere changes from completely transparent to semi-transparent and finally will become an opaque dusty surface. As τ increases, the sphere becomes smoother and softer, especially near the contour. This is consistent with the effects of dusty opaque surfaces since our model subsumes Blinn's dust model. However, we also capture the transmission effects of the dust layer on the glass sphere.

Looking Through a Window in Daytime and Nighttime: Figure 14 shows a view through a window of a room. The outside scene is from the Weather and Illumination Database [NWN02] with lighting changing over time (from morning to night). Inside the room, we have a fixed environment light. The contamination pattern is composed of dried water streaks (dirt) in the left of the window, smudges and fingerprints (lipids) in the right, and a very thin layer of dust. As shown, against the sky the contaminant pattern looks darker because of attenuation; while against the building (or in the shadow of the building), the contamination pattern looks brighter because of scattering. Moreover, when viewing the window at different times of day, with differ-

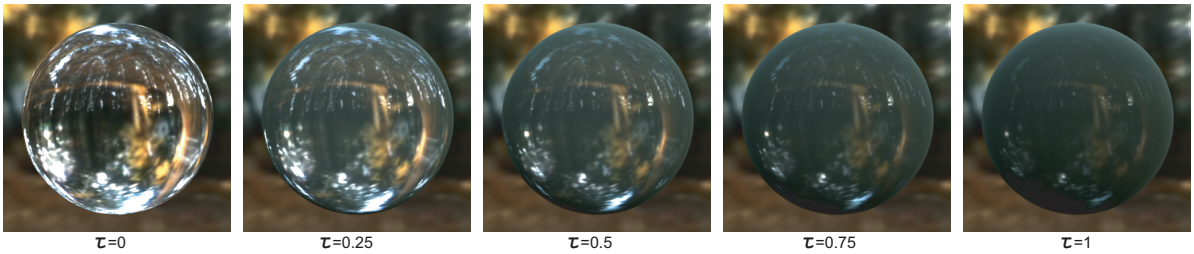

Figure 13: *A glass sphere rendered with different thicknesses of a uniform layer of dust. As the optical thickness increases (from left to right), both the transmission and the reflection become smoother and give the sphere a more velvety appearance, especially near the boundary*

Figure 14: *A contaminated window rendered with a background that changes with time of day. Note how the contaminants appear very different for the different illuminations of the background.*

ent types of illumination, the contaminant pattern generates various effects, as predicted by our model in Fig. 8.

Monitor On/Off: Figure 15 shows a monitor screen with contaminant when it is turned on and off. As predicted in Sec. 4, when turning on the monitor, we cannot see the contaminants most of the time; when turning off the monitor, details of the contaminants are visible to us. Moreover, as either view or illumination moves more toward grazing angles, the *effective* optical thickness of the contaminant layer increases and exaggerates scattering effects.

Dirty Cognac Glass: Figure 16 shows a cognac glass covered with a uniform layer of contaminant while the optical thickness of the contaminant increases. We render the results with photon mapping. The body of the cognac glass has a similar appearance as the glass sphere example, while the base of the cognac and the caustics show interesting changes due to the scattering and the attenuation of the contaminant. In Fig. 17, we show a cognac glass with a textured contaminant rendered with and without scattering. Notice the subtle visual effects produced by the scattering of the contaminant, including the vertical "shadows" on the glass body, the contrast reversals of the contaminant against the background, and the increased scattering effects at grazing angles.

6.2. Creating Contamination Effects on Photographs

Besides rendering 3D scenes, we also show that our model can be used as an "effects filter" for 2D photographs to add the appearance of contamination to images of clean transparent surfaces.

Figure 15: *A monitor screen rendered with dust and fingerprints. The contaminants become more clearly visible when the monitor is off. Their brightness increases as the viewing angle approaches the grazing angle.*

Scattering on a Camera Lens: Contaminants on camera lenses will scatter lights and generate effects such as lens flare from stray lights and blurring, as seen in Fig. 1c. Based

Figure 16: *A cognac glass rendered with different thicknesses of a uniform dust layer (increasing from left to right). The caustics and the base of the glass become dimmer and smoother as the dust thickness increases.*

Figure 17: *A cognac glass rendered with stains. The glass is rendered (a) with and (b) without scattering from the stains.*

on our model, we can use an image taken with a clean lens, such as Fig. 18a, and composite it as if it were taken with a dirty lens, as shown in Fig. 18b. The texture of the contamination pattern is created to be similar as that in Fig. 1c. Chromatic effects of lenses could also be added by assigning different refraction indices for R/G/B channels in the model. The same method can be applied to other 2D images. For example, Fig. 19c shows an image rendered as if it were taken through a glass that had been sprayed by sea water. Figures 19a, 19b show the original image and the pattern of salt deposits used for rendering.

Contaminating Clean Transparent Surfaces: As shown in Fig. 20, our goal is to make the window region in the input photograph dirty. We first estimate the 3D positions of the window plane and camera from the four corner points of the window. The outside illumination is assumed to be the image intensity in the window region synthesized and mapped onto the hemisphere. Using our BRDF and BTDF, we can compute the image intensity in the regions of the window with contamination. In Fig. 20, (a) is the photograph with a clean window [DD02], (b) is the estimation of the illumination outside and the 3D positions for the window and camera, (c) is a synthesized contaminant pattern used for rendering, and (d) is the final composite result. Notice the brighter appearance of the window on the bottom right and the darker appearance in the top regions in (d). Simple alpha-blending could not generate these effects.

Figure 18: *Compared with the real photograph Fig. 1(c), our model can be used to modify (a) a photograph of the scene taken with a clean camera lens to create the effects of (b) an image as if it were taken with a dirty camera lens.*

7. Conclusion

Contamination such as dust, dirt, and lipids create a weathered appearance on transparent objects due to scattering. In this paper, we have presented a comprehensive study for rendering these scattering effects. By modeling the contaminant as an optically-thin layer of a scattering medium, we construct an analytic BRDF/BTDF model based on pre-existing results in computer graphics and radiative transport theory, which accurately captures most of the canonical visual effects of contaminated transparent surfaces and allows efficient rendering. We also propose novel methods to measure both the thickness patterns and scattering parameters for various kinds of contamination in the real world. We show that our model and the measurements can be used for rendering of 3D scenes and 2D photographs to create a photorealistic appearance for contaminated transparent surfaces. An interesting area for future work is to extend our model to the rendering of contaminated translucent materials, such as lipids on skin, dust on marble, and dirt on transparent vessels holding participating media (e.g., wine and various other liquids). Moreover, the BRDF/BTDF model may also be helpful in solving inverse problems, such as removing contamination effects in photographs, e.g., “cleaning” dirty glass.

Acknowledgements: We thank Srinivasa Narasimhan for useful discussion about scattering parameter measurement and Craig Donner for the cognac glass mesh. This work was supported in part by NSF grants #0325867, #0446916 and

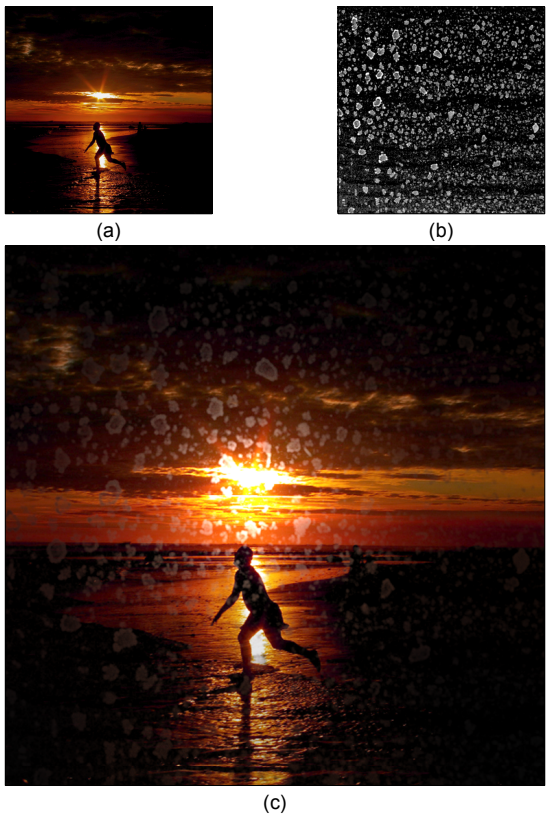

Figure 19: *The modified image in (c) was created using the real image in (a) and the measured salt deposit pattern shown in (b).*

#0541259, ONR grants N00014-05-1-0188 and N00014-07-1-0900, and a Sloan research fellowship.

References

[Bli82] BLINN J.: Light reflection functions for simulation of clouds and dusty surfaces. *Computer Graphics 16*, 3 (1982), 21–29.

[BPMG04] BOSCH C., PUEYO X., MERILLOU S., GHAZANFARPOUR D.: A physically-based model for rendering realistic scratches. *Eurographics 23*, 3 (2004), 361–370.

[Cha60] CHANDRASEKHAR S.: *Radiative Transfer*. Dover Publications, New York, 1960.

[CPW90] CHEONG W., PRAHL S., WELCH A.: A review of the optical properties of biological tissues. *IEEE Journal of Quantum Electronics 26*, 12 (1990), 2166–2185.

[DD02] DURAND F., DORSEY J.: Fast bilateral filtering for the display of high-dynamic-range images. *ACM Transactions on Graphics (SIGGRAPH) 21*, 3 (2002), 257–266.

[DEWJ*99] DORSEY J., EDELMAN A., WANN JENSEN H., LEGAKIS J., PEDERSON H.: Modeling and rendering of weathered stone. In *SIGGRAPH* (1999), pp. 225–234.

[DH96] DORSEY J., HANRAHAN P.: Modeling and rendering of metallic patinas. In *SIGGRAPH* (1996), pp. 387–396.

[DH00] DORSEY J., HANRAHAN P.: Digital materials and virtual weathering. *Scientific American 282*, 2 (Feb. 2000), 46–53.

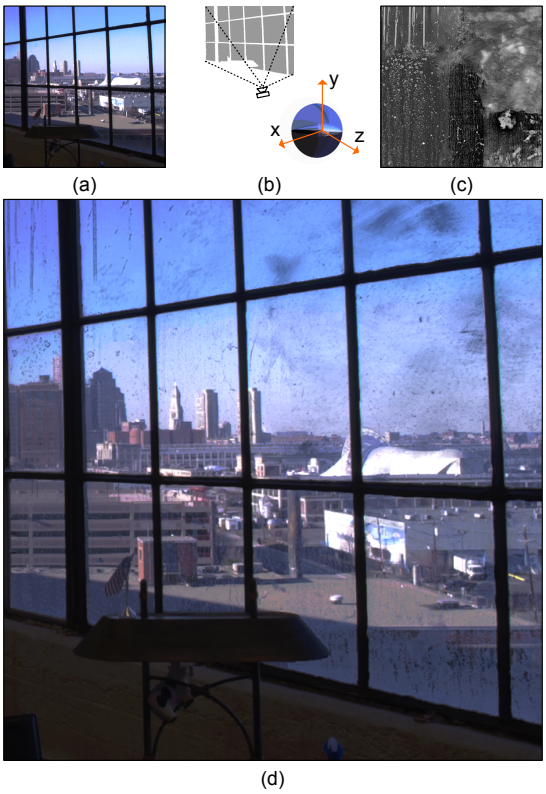

Figure 20: *Making clean windows in real photographs dirty. (a) The original photograph. (b) Using the straight lines on the photograph and the appearance of the scene beyond the window, approximations for the pose of the camera and the background illumination were obtained. This information was used with a mosaic of various contamination patterns in (c) to render the final image in (d).*

[DPH96] DORSEY J., PEDERSON H., HANRAHAN P.: Flow and changes in appearance. In *SIGGRAPH* (1996), pp. 411–420.

[Dra03] DRAINE B.: Interstellar dust grains. *Annual Review of Astronomy and Astrophysics 41* (2003), 241–287.

[EF01] EFROS A., FREEMAN W.: Image quilting for texture synthesis and transfer. In *SIGGRAPH* (Los Angeles, CA, August 2001), pp. 341–346.

[EKM01] ERSHOV S., KOLCHIN K., MYSZKOWSHI K.: Rendering pearlescent appearance based on paint-composition modeling. *Eurographics 20*, 3 (2001), 227–238.

[GTR*06] GU J., TU C., RAMAMOORTHI R., BELHUMEUR P., MATUSIK W., NAYAR S.: Time-varying surface appearance: Acquisition, Modeling and Rendering. *ACM TOG (SIGGRAPH) 25*, 3 (2006), 762–771.

[HK93] HANRAHAN P., KRUEGER W.: Reflection from layered surfaces due to subsurface scattering. *SIGGRAPH* (1993), 165–174.

[HM03] HAKIM A., MCCORMICK N.: Ocean optics estimation for absorption, backscattering, and phase function parameters. *Applied Optics 42*, 6 (2003), 931–938.

[HW95] HSU S., WONG T.: Simulating dust accumulation. *IEEE Computer Graphics & Applications 15*, 1 (January 1995), 18–22.

[Ish78] ISHIMARU A.: *Wave Propagation and Scattering in Random Media*. IEEE Press, New York, 1978.

[JDJ06] JOSHI N., DONNER C., JENSEN H.: Non-invasive scattering anisotropy measurement in turbid materials using non-normal incident illumination. *Optics Letters 31* (2006), 936–938.

[Jen01] JENSEN H.: *Realistic Image Synthesis Using Photon Mapping*. A K Peters, Ltd., Wellesley, MA, 2001.

[JMLH01] JENSEN H., MARSCHNER S., LEVOY M., HANRAHAN P.: A practical model for subsurface light transport. *SIGGRAPH* (2001), 511–518.

[KP03] KOENDERINK J., PONT S.: The secret of velvety skin. *Machine Vision and Applications 14* (2003), 260–268.

[LGR*05] LU J., GEORGHIADES A., RUSHMEIER H., DORSEY J., XU C.: Synthesis of material drying history: Phenonmenon modeling, transfering, and rendering. *Eurographics Workshop on Natural Phenomena* (2005), 7–16.

[MDG01] MERILLOU S., DISCHLER J.-M., GHAZANFARPOUR D.: Corrosion: simulating and rendering. In *Graphics Interface* (Ottawa, Canada, 2001), pp. 167–174.

[Mil94] MILLER G.: Efficient algorithms for local and global accessibility shading. In *SIGGRAPH* (1994), pp. 319–326.

[NGD*06] NARASIMHAN S., GUPTA M., DONNER C., RAMAMOORTHI R., NAYAR S., JENSEN H.: Acquiring scattering properties of participating media by dilution. *ACM Transactions on Graphics (SIGGRAPH) 25*, 3 (2006), 1003–1012.

[NWN02] NARASIMHAN S., WANG C., NAYAR S.: All the Images of an Outdoor Scene. In *European Conference on Computer Vision (ECCV)* (May 2002), vol. III, pp. 148–162.

[PH00] PHARR M., HANRAHAN P.: Monte carlo evaluation of non-linear scattering equations for subsurface reflection. *SIGGRAPH* (2000), 75–84.

[PH04] PHARR M., HUMPHREYS G.: *Physically Based Rendering: From Theory to Implementation*. Morgan Kaufmann, 2004.

[PPD01] PAQUETTE E., POULIN P., DRETTAKIS G.: Surface aging by impacts. *Graphics Interface* (2001), 175–182.

[SFMM01] SCHIMINOVICH D., FRIEDMAN P., MARTIN C., MORRISSEY P.: The narrow-band ultraviolet imaging experiment for wide-field surveys (nuviews)-i: Dust scattered continuum. *The Astrophysical Journal 563* (2001), 161–180.

[SSR*06] SUN B., SUNKAVALLI K., RAMAMOORTHI R., BELHUMEUR P., NAYAR S.: Time-varying BRDFs. *Eurographics Workshop on Natural Phenomena* (2006), 15–23.

[Sta01] STAM J.: An illumination model for a skin layer bounded by rough surfaces. *in Rendering Techniques'01, Proceedings of the 12th Eurographics Workshop on Rendering* (2001), 39–52.

[Sto90] STOVER J.: *Optical scattering: measurement and analysis*. McGraw-Hill, New York, 1990.

[WDE*97] WEST R., DOOSE L., EIBL A., TOMASKO M., MISHCHENKO M.: Laboratory measurements of mineral dust scattering phase function. *Journal of Geophysical Research 102*, D14 (1997), 16871–16882.

[WTL*06] WANG J., TONG X., LIN S., PAN M., WANG C., BAO H., GUO B., SHUM H.: Appearance manifolds for modeling time-variant appearance of materials. *ACM TOG (SIGGRAPH) 25*, 3 (2006), 754–761.

Appendix

In this appendix, we list some formulae and definitions used in Secs. 3 and 5.

BRDF/BTDF Model When $\omega_i \cdot N < 0$: In the case of $\omega_i \cdot N < 0$, the light is incident from the glass to the air (Fig. 4b), we need to change the derived components in Eqs. 1-6 accordingly and the corresponding BRDF and BTDF models need to be changed as follows:

$$\begin{aligned} f_r(\omega_i,\omega_r) &= \frac{\delta(\omega_i,\omega_r)}{\mu_i}\left(F_{23}+T_{32}T_{23}F_{12}e^{-\tau(\frac{1}{\mu_i'}+\frac{1}{\mu_r'})}\right) \\ &+ \frac{T_{32}T_{23}\mu_i'}{(\mu_i'+\mu_r')\mu_i}\left(1-e^{-\tau(\frac{1}{\mu_i'}+\frac{1}{\mu_r'})}\right)\varpi_0 p(\pi-\theta_i'-\theta_r') \\ &+ \frac{T_{32}T_{23}F_{12}\mu_i'}{(\mu_i'-\mu_r')\mu_i}\left(e^{-\tau/\mu_i'}-e^{-\tau/\mu_r'}\right)e^{-\tau/\mu_i'}\varpi_0 p(\theta_i'-\theta_r'), \end{aligned}$$

and

$$\begin{aligned} f_t(\omega_i,\omega_t) &= \frac{\delta(\omega_i',\omega_t')}{\mu_i}T_{12}T_{23}e^{-\tau/\mu_i'} \\ &+ \frac{T_{12}T_{23}\mu_i'}{(\mu_i'-\mu_t')\mu_i}\left(e^{-\tau/\mu_i'}-e^{-\tau/\mu_t'}\right)\varpi_0 p(\theta_i'-\theta_t'), \end{aligned}$$

where ω_i', ω_r', and ω_t' should also be computed with different refractive indexes.

Changes in the Models for Thin Transparent Slab: Specifically, as shown in Fig. 6, for the case $\omega_i \cdot N > 0$ (i.e., the incident light first hits the contaminant layer and then transmits into the transparent slab and finally goes out to the air), for the BRDF, $L_r^{(1)}$ and $L_r^{(3)}$ are unchanged. For $L_r^{(2)}$ and $L_r^{(4)}$, we need to replace F_{23} by $F_{23} + T_{23}T_{32}F_{31}$ in Eq. 2 and Eq. 4, since we need to take into account that a part of the transmitted light in the slab will be reflected back into the contaminant layer (the ray marked with $\star$ in Fig. 6). For the BTDF, both $L_t^{(1)}$ and $L_t^{(2)}$ in Eq. 5 and Eq. 6 need to be multiplied by an additional term T_{31} when the refracted rays come out from the slab to the air. The directions of the refracted rays, ω_t', also need to be changed accordingly.

Derivation of Eq. 8 for Scattering Measurement: As shown in Fig. 9b, for a point (x,y) on the Lambertian board, its outgoing radiance is proportional to the irradiance $L_c(x,y) = \rho \cdot E(x,y)$, where ρ is the albedo of the board, and the irradiance $E(x,y)$ can be computed as $E(x,y) = L_t^{(2)}(\omega_t)\cos\theta\, d\omega_t$, where $L_t^{(2)}(\omega_t)$ is the outgoing radiance of the contaminant due to scattering of the incident beam, and the solid angle $d\omega_t$ is given by $d\omega_t = \frac{dA_p\cos\theta}{(d/\cos\theta)^2}$, where dA_p is the area of the contaminant layer illuminated by the beam and d is the distance from the slab to the board. Based on these and Eq. 6 in Sec. 3 for $L_t^{(2)}(\omega_t)$, we can derive that (note that the incident direction ω_i is perpendicular to the slab and thus $\cos\theta_i = \cos\theta_i' = 1$):

$$I(x,y) \propto L_c(x,y) \propto p(\theta;g)\cdot\frac{e^{-\tau}-e^{-\tau/\cos\theta}}{1-\cos\theta}\cdot\cos^4\theta,$$

where we approximate the angle of the refracted ray inside the contaminant layer as θ. From this equation, we fit the phase function $p(\theta;g)$ with a nonlinear optimization algorithm to estimate g.